Resonant soft-x-ray emission spectroscopy of surface adsorbates: Theory, computations, and measurements of ethylene and benzene on Cu(110)

Luciano Triguero, Yi Luo, and Lars G. M. Pettersson
FYSIKUM, University of Stockholm, Box 6730, S-113 85 Stockholm, Sweden

Hans Ågren
Institute of Physics and Measurement Technology, Linköping University, S-58183 Linköping, Sweden

Peter Väterlein, Martin Weinelt, Alexander Föhlisch, Jörgen Hasselström, Olof Karis, and Anders Nilsson
Department of Physics, Uppsala University, Box 530, S-751 21 Uppsala, Sweden

(Received 18 May 1998)

Soft-x-ray emission spectra from C_2H_4/Cu(110) and C_6H_6/Cu(110) have been obtained for two excitation energies, resonant and nonresonant, and resolved in all three spatial components (x,y,z). The one-step theory for resonant soft x-ray spectroscopy and Raman scattering is extended to adsorbates on metal surfaces and is implemented within a density-functional theory framework. The calculations are performed for ethylene and benzene chemisorbed on Cu(110) using cluster models (up to 86 Cu atoms) of the metal surface; the calculations are performed for both resonant and nonresonant excitation with the focus on the polarization and symmetry selectivity and the role of channel interference. The molecular mirror plane symmetry is maintained for the chemisorbed system, and for the generated core hole, which leads to an energy-dependent symmetry and polarization selectivity in the emission process. The calculations and experiment show good agreement both with regard to intensities and energy positions of the peaks. [S0163-1829(99)05804-X]

I. INTRODUCTION

X-ray emission spectroscopy (XES) is complementary to x-ray absorption spectroscopy (XAS) in that it probes the electronic structure of the occupied rather than of the unoccupied levels. It shares with XAS the property of being symmetry, orientational, and polarization selective and of probing local electronic structure of certain atomic subsymmetries. However, since the final state contains only a valence hole the XE spectroscopy relates more directly to chemistry and physics of the ground-state species. For *resonantly* excited x-ray spectra, or resonant inelastic x-ray scattering (RIXS), these features are strongly enhanced, and qualitatively different, because the selective excitation of a particular intermediate core-excited state of a certain symmetry prepares the emission both with respect to symmetry and polarization. A further, major, difference with respect to the nonresonant case, is the possibility of a channel interference effect, which is of great importance for the symmetry selection and the polarization dependence as well as for the total emission cross section in the resonant case. The tuning of the incoming x-ray radiation to the discrete resonances of the target molecule may thus lead to scattering spectra that show very specific polarization and symmetry dependences which provide direct evidence of symmetry assignments of the participating electronic levels.

The main features associated with resonant x-ray emission spectra can be understood from second-order perturbation theory between light and matter, as described by the Kramers-Heisenberg equation[1] for the x-ray scattering amplitude. The applications of this equation, which implements the so-called one-step picture, have been much studied for free atoms[2,3] and molecules,[4–6] and also for crystalline solids.[7–14] Several experimental and computational applications have been performed to a group of representative molecules with random orientations such as benzene, chlorofluoromethanes, aniline, and C_{60}.[6,15–17] While this theory certainly is expected to carry over to surfaces and surface adsorbates, little is yet known about its actual consequences for resonant x-ray emission spectra of such systems. An evident difference with respect to free molecules is the fact that orientational averaging of the sample is no longer appropriate, making the orientational and polarization dependences so much sharper. Dipole and momentum selection rules, appropriate for gases and solids, respectively, will have a different meaning, due to the quasicontinuous set of levels that often show up for surface adsorbate systems. One can anticipate that, just as for gas phase systems and solids, there is a strong connection between the channel interference and the actual observation of the dipole selection rules, something that is verified in the present work. Towards the harder x-ray region, $\simeq$1000 eV and beyond, one might anticipate a close connection between the channel interference and the selection rules, on the one hand, and the photon phase factors and the Bragg conditions on the other, making the scattering cross sections strongly anisotropic and oscillatory.[18] Different dephasing mechanisms, such as orientational disorder, vibrational motion and vibronic coupling, may destroy the interchannel coherence and eliminate the selection rules.[18]

The present work combines theory, computations, and experiment in an effort to understand resonant soft-x-ray emission spectra—or soft-x-ray Raman spectra—from surface adsorbates, using the experimental and theoretical spectra of

ethylene and benzene on the copper (110) surface as particular test cases.

The theoretical effort is based on a group theoretical formulation for the one-step resonant x-ray emission cross section of randomly oriented molecules which applies to any type of polarization for the absorbed and emitted photons (linear, circular, or elliptical) and for any molecular point group,[5] and that here is applied to samples with fixed orientation. In addition to the generality of the theory, a particular advantage with this formulation is that the information concerning polarization, molecular orientation, and intrinsic molecular properties are separated—and so can be analyzed—in three different factors.

On the computational side we use methods based on gradient corrected density-functional theory (DFT), that recently were developed for the calculations of nonresonant x-ray emission spectra of surface adsorbates,[19] and explore how they apply to resonant spectra. The surface is modelled by clusters of different size with the largest cluster consisting of 86 copper atoms, and both the variation of the spectral features with cluster size, and the general cluster convergence, are important issues in the present work.

On the experimental side we make use of the fact that polarized synchrotron x-ray radiation can be tuned to the discrete resonances of surface adsorbed targets, and that sufficient intensity thereby is gained to observe the scattering spectra with specific angular and symmetry dependences.[20,21] Recent experiments using x-ray emission spectroscopy have examined the spectra of ethylene adsorbed on Cu(110) and of benzene on Cu(110) and Ni(100).[22] These experiments show small, but significant differences between resonant and nonresonant excitation in the case of chemisorbed ethylene, while in the case of benzene chemisorbed on Cu(110) restricted selection rules are found to apply to the resonant x-ray emission spectra.

In the following, we first outline a second-order perturbation theory approach to resonant x-ray emission spectra of surface adsorbates, which is generally applicable in the soft-x-ray regime below 1000 eV (Sec. II). In Sec. III we discuss the computational approach and give some details on the methods used (density functionals and basis sets) and of the chosen clusters and the adsorbate structure. This is followed by a description of the experiment (Sec. IV), and a section (Sec. V) where the experimental and computational results for ethylene and benzene on copper (110) are presented and discussed. In the last Sec. VI, we summarize the findings of the present work.

II. THEORY FOR POLARIZED RESONANT X-RAY EMISSION FROM ADSORBED MOLECULES

The general theory for symmetry selective resonant x-ray emission from randomly oriented molecules has been presented in several previous studies (see Refs. 4–6, 23) and has been applied to molecular systems as different as diatomic molecules,[24] substituted benzenes[16,25] and fullerenes.[17] The formalism is based on second-order perturbation theory for the interaction between light and matter, leading to the Kramers-Heisenberg dispersion formula, that describes resonant inelastic x-ray scattering.

If only the resonant part of the scattering process is taken into account then the spectral and polarization properties of RIXS are guided by the double differential cross section,

$$\frac{d^2\sigma}{d\omega' d\Omega} = \sum_{\nu} \sum_{n} \frac{\omega'}{\omega} |F_{\nu n}(\omega)|^2 \delta(\omega - \omega' - \omega_{\nu n}), \quad (1)$$

where the final-state lifetime broadening $\Gamma_{\nu n}$ for the optically excited final state is neglected, $\Gamma_{\nu n}=0$. Assuming a finite width γ of the distribution of the incoming photons $\Phi(\omega-\omega_0)$ the convoluted RIXS cross section becomes

$$\sigma(\omega',\omega_0) = \int d\omega \frac{d^2\sigma}{d\omega' d\Omega} \Phi(\omega-\omega_0)$$

$$= \sum_{\nu n} \frac{\omega'}{\omega} |F_{\nu n}(\omega)|^2 \Phi(\omega' + \omega_{\nu n} - \omega_0), \quad (2)$$

where ω_0 denotes the center of the frequency distribution for the incoming photons. From this expression, and in accordance with the energy conservation law reflected by the $\delta(\omega-\omega'-\omega_{\nu n})$ function, it follows that the frequency ω' of the emitted x-ray photons has a Raman related shift (Stokes shift) into the long-wave region relative to the frequency ω of the absorbed photon

$$\omega = \omega' + \omega_{\nu n}. \quad (3)$$

Here $\omega_{\nu n}=E(n^{-1}\nu)-E_0$ is the frequency for optical excitation $n\rightarrow\nu$ from valence level n to unoccupied level ν and is equal to the difference between the (total) energies $E(n^{-1}\nu)$ and E_0 of the excited $|n^{-1}\nu\rangle$ and ground $|0\rangle$ molecular states.

The RIXS total amplitude is a sum over channel amplitudes. (Atomic units are used throughout. In these units $\hbar = m_e = e = 1$, and the fine-structure constant $\alpha = 1/137$.)

$$F_{\nu n}(\omega) = \sum_{k} f^k_{\nu n}(\omega), \quad (4)$$

$$f^k_{\nu n}(\omega) = \alpha \omega_{\nu k} \omega_{nk}(\nu) \frac{(\mathbf{e}_1^* \mathbf{d}_{\nu k})[\mathbf{e}_2 \mathbf{d}_{kn}(\nu)]}{\omega - \omega_{\nu k} + i\Gamma_{\nu k}}. \quad (5)$$

$\mathbf{d}_{\nu k}=\langle 0|\mathbf{p}|k^{-1}\nu\rangle$ and $\mathbf{d}_{kn}(\nu)=\langle k^{-1}\nu|\mathbf{p}|n^{-1}\nu\rangle$ are the transition dipole matrix elements governing the x-ray absorption ($k\rightarrow\nu$) and emission ($n\rightarrow k$) processes, respectively. Indices k, n, and ν denote levels defined by core, occupied, and unoccupied molecular orbitals, respectively. $\omega, \mathbf{e}_1$ denote, respectively, the frequency and polarization vectors of the incoming photons, while $\mathbf{e}_2$ is the polarization vector of the emitted photons.

The resonant frequency, $\omega_{\nu k}$, for excitation from core level k to unoccupied level ν is given by $\omega_{\nu k}=E(k^{-1}\nu)-E_0$, while the frequency shift, $\omega_{nk}(\nu)$, between scattered and incoming photons for intermediate level ν, core level k, and final valence hole in orbital n is given by $\omega_{nk}(\nu)=E(k^{-1}\nu)-E(n^{-1}\nu)$. Finally, $\Gamma_{\nu k}$ is the half-width at half-maximum (HWHM) of the x-ray absorption line $k\rightarrow\nu$. The index ν in $\mathbf{d}_{kn}(\nu)$ and $\omega_{nk}(\nu)$ indicates possible differential screening effects from the particular level ν on the decay of electrons from various occupied levels n to the inner shell k.

The most prominent selection rule in RIXS is that of parity. This, as the other selection rules, is controlled by the

parameter $d^{\beta}_{\nu k} d^{\gamma}_{kn}(\nu)$ involving the product of transition dipole components β,γ (corresponding to *x,y,z* Cartesian directions) for the excitation and emission processes. For instance, if the occupied and unoccupied molecular orbitals (MO's) involved in the transitions have opposite parity ($u-g$ or $g-u$) then $d^{\beta}_{\nu k} d^{\gamma}_{kn}(\nu) \equiv 0$, and the transition is forbidden. However, for strongly chemisorbed species such a parity selection can be expected to be broken due to the presence of the surface. Therefore, in the analysis of RIXS spectra for surface adsorbates the symmetry selection rule would be expected to be more relevant. This is obtained by simply investigating the product of irreducible representations $\Gamma_{\nu} \times \Gamma_{\alpha} \times \Gamma_{\beta} \times \Gamma_{n}$, where ν and n denote unoccupied and occupied orbitals, and α and β the appropriate transition dipole components; this product must contain the totally symmetric representation for a transition to become allowed. This general rule is, however, by itself not very useful for extracting information from a measurement, neither concerning symmetries nor orientations. Instead, one must find a formalism that directly links the photon propagation and polarization directions of the incoming and outgoing photons to obtain this information.

We consider in this work coordinate systems that are given by Fig. 1. The polarization vectors are expressed in the laboratory coordinates *X*, *Y*, and *Z*, while the transition dipole matrix elements are given in the molecular coordinates *x*, *y*, and *z*, see Fig. 1. The transition dipole moments $d_{\nu k}$ and d_{kn} can be expressed in laboratory coordinates through the directional cosine transformation $T^{X}_{k} = T^{x}_{k} t_{xX} + T^{y}_{k} t_{yX} + T^{z}_{k} t_{zX} = T^{\alpha}_{k} t_{\alpha X}$, where the repeated Greek index α implies summation over the values *x*, *y* and *z*; e.g., t_{xX} is the cosine of the angle between the *x* axis of the molecular coordinate system and the *x* axis of the laboratory coordinate system. The eight other directional cosines $t_{xY}, t_{xZ}, t_{yX}, \ldots$ are named similarly; the general direction cosine will in the following be denoted $t_{\alpha A}$ using a Greek letter for the molecular axis and a capital italic letter for the laboratory axis. Using these transformations the total *x*-ray scattering amplitude [Eq. (4)] is obtained as

$$F_{\nu n}(\omega) = \alpha \sum_{k} \omega_{\nu k} \omega_{nk}(\nu) \frac{d^{\beta}_{\nu k} t_{\beta A} e^{*}_{1A} d^{\gamma}_{kn}(\nu) t_{\gamma B} e_{2B}}{\omega - \omega_{\nu k} + i\Gamma_{\nu k}} \quad (6)$$

or rearranging as

$$F_{\nu n}(\omega) = (t_{\beta A} t_{\gamma B})(e^{*}_{1A} e_{2B}) F^{\beta\gamma}_{\nu n}(\omega), \quad (7)$$

where we define $F^{\beta\gamma}_{\nu n}(\omega)$ as

$$F^{\beta\gamma}_{\nu n}(\omega) = \alpha \sum_{k} \omega_{\nu k} \omega_{nk}(\nu) \frac{d^{\beta}_{\nu k} d^{\gamma}_{kn}(\nu)}{\omega - \omega_{\nu k} + i\Gamma_{\nu k}} \quad (8)$$

and this quantity corresponds to the RIXS transition element. It can be seen that $F^{\beta\gamma}_{\nu n}$ is a tensor of second rank (in the following we will for simplicity drop the explicit dependence on the excitation frequency ω). The quantity $|F_{\nu n}|^2$ is thus written as

$$|F_{\nu n}|^2 = (e^{*}_{1A} e_{2B} e_{1R} e^{*}_{2S})[t_{\beta A} t_{\gamma B} t_{\rho R} t_{\sigma S}](F^{\beta\gamma}_{\nu n} F^{\rho\sigma *}_{\nu n}). \quad (9)$$

All polarization information is now collected in the first factor, all molecular information in the last factor, and all orientational information in the middle factor. Both the first and last factors in Eq. (9) are Cartesian tensors of fourth rank. For randomly oriented molecules, like molecules in the gas phase, an orientational averaging over three dimensions must be employed; a detailed analysis for the RIXS spectra of gas phase molecules can be found in (Refs. 5,17). For adsorbates, the orientational arrangements of the molecules are by definition asymmetric and averaging over directions can in the general case not be performed; for certain cases directions in the surface plane will be equivalent, but this is not always true. Therefore, different polarization dependence of the RIXS spectra can be expected for different systems. In the present paper, the RIXS spectra of absolutely ordered adsorbates will be studied in detail.

Equation (7) can be rearranged as

$$F_{\nu n} = \sum_{\beta\gamma} L_{1\beta} L_{2\gamma} F^{\beta\gamma}_{\nu n}, \quad (10)$$

where

$$L_{1\beta} = \sum_{A} e^{*}_{1A} t_{\beta A}, \quad (11)$$

$$L_{2\gamma} = \sum_{A} e_{2A} t_{\gamma A}, \quad (12)$$

in which the summation has been reintroduced. $L_{1\beta}$ and $L_{2\gamma}$ are the direction cosines of polarization vectors $\mathbf{e}_1$ and $\mathbf{e}_2$ in the molecular frame. Therefore

$$|F_{\nu n}|^2 = \left| \sum_{\beta\gamma} L_{1\beta} L_{2\gamma} F^{\beta\gamma}_{\nu n} \right|^2. \quad (13)$$

The total cross section is given by

$$\sigma(\omega', \omega_0) = \sum_{\nu n} \frac{\omega'}{\omega} \left| \sum_{\beta\gamma} L_{1\beta} L_{2\gamma} F^{\beta\gamma}_{\nu n} \right|^2 \Phi(\omega' + \omega_{\nu n} - \omega_0). \quad (14)$$

The spectral shape for RIXS spectra of randomly oriented molecules has been discussed in Refs. 4,5; similar conclusions regarding spectral shapes as in the cited works can be drawn for RIXS of adsorbed molecules.

For adsorbed molecules with degenerate and quasidegenerate core orbitals, it is a good approximation to assume $\omega_{\nu,k} = \omega_{\nu,0}$ for all core MO's *k*. One could furthermore assume that for a fixed ν MO, the damping factor (core excited state lifetime broadening) $\Gamma_{\nu k}$ is the same for all core-excited states (core MO's *k*), i.e., that $\Gamma_{\nu k} = \Gamma_{\nu 0}$. Equation (8) can thus be written as

$$F^{\beta\gamma}_{\nu n} = \frac{1}{\omega - \omega_{\nu 0} + i\Gamma_{\nu 0}} \sum_{k} \alpha \omega_{\nu k} \omega_{nk} d^{\beta}_{\nu k} d^{\gamma}_{kn} = \frac{\left(\frac{\Gamma_{\nu 0}}{\pi}\right)^{1/2}}{\omega - \omega_{\nu 0} + i\Gamma_{\nu 0}} D^{\beta\gamma}_{\nu n} \quad (15)$$

and

$$|F_{\nu n}|^2=\frac{\Gamma_{\nu 0}}{\pi[(\omega-\omega_{\nu 0})^2+\Gamma_{\nu 0}^2]}\left|\sum_{\beta\gamma} L_{1\beta}L_{2\gamma}D_{\nu n}^{\beta\gamma}\right|^2$$
$$=\Delta(\omega-\omega_{\nu 0},\Gamma_{\nu 0})|D_{\nu n}|^2. \quad (16)$$

Finally, the cross section can be written as

$$\sigma(\omega',\omega_0)=\sum_{\nu n}\sigma_{\nu n}(\omega',\omega_0) \quad (17)$$

and

$$\sigma_{\nu n}(\omega',\omega_0)=\frac{\omega'}{\omega}|D_{\nu n}|^2\Delta(\omega-\omega_{\nu 0},\Gamma_{\nu 0})\Phi(\omega-\omega_0). \quad (18)$$

The spectral shape of the RIXS cross section is thus determined by the product of the $\Delta(\omega-\omega_{\nu 0},\Gamma_{\nu 0})$ and the $\Phi(\omega-\omega_0)$ functions. Such a spectral shape leads to Raman effects such as linear dispersion, resonance narrowing, and Stokes doubling.[17]

In the following, we will discuss several typical systems in terms of simplified few-states models. We will assume excitation into a strongly absorbing π system, assume that this is orthogonal to the substrate and that the excitation thus takes place at grazing incidence with the polarization vector of the incident photon parallel to the direction vector of the adsorbates, i.e., $L_{1\beta}=\delta_{Zz}$. Furthermore, a δ function is assumed for the spectral lineshape of the incoming photon, i.e., $\Phi(\omega-\omega_0)=\delta_{\omega,\omega_0}$.

A. A single core orbital

For a process with one core orbital involved, one has

$$|F_{\nu n}|^2=\Delta(\omega-\omega_{\nu 0},\Gamma_{\nu 0})|I_{\nu k}^z|^2\left|\sum_{\gamma} L_{2\gamma}I_{kn}^{\gamma}\right|^2, \quad (19)$$

where $I_{ik}^{\beta}=\alpha^{1/2}\omega_{ik}d_{ik}^{\beta}$ $(i=\mu,n;\quad \beta=z,\gamma)$,

$$\sigma(\omega',\omega_k)=\sum_{\nu}\Delta(\omega_0-\omega_{\nu k},\Gamma_{\nu k})|I_{\nu k}^z|^2\sum_n\left|\sum_{\gamma} L_{2\gamma}I_{kn}^{\gamma}\right|^2, \quad (20)$$

It clearly shows that, in this case, the absorption and emission processes are completely decoupled. The spectral shape of emission should not depend on the excitation energy within a frozen orbital picture; thus, an observed difference between two emission spectra excited at two different excitation energies should provide information about the energy dependence of the relaxation of the core excited state. This formula also corresponds to the traditional two-step model (TSI) in which only the decay from the valence orbitals to the core orbitals is considered.

B. Polarization selective excitation: Two (near-degenerate) core orbitals of different symmetry

The (formal) symmetry of adsorbates is always reduced relative to the gas phase due to the presence of the surface and in the example below we will assume a system with C_{2v} symmetry as an example. The two initial (near-degenerate) core orbitals, k_1 and k_2, are assumed to have symmetries a_1 and b_1, respectively. Since the polarization vector of the incoming photon is along the z direction (grazing incidence), only unoccupied orbitals with symmetries a_1 and b_1 will be involved in the absorption processes. Therefore, we will here only consider two groups of unoccupied orbitals, ν_1 and ν_2 with symmetries a_1 and b_1, respectively. One thus obtains

$$\sigma(\omega',\omega_0)=\sum_{\nu_1}\Delta_1|I_{\nu_1k_1}^z|^2\sum_n\left|\sum_{\gamma} L_{2\gamma}I_{k_1n}^{\gamma}\right|^2$$
$$+\sum_{\nu_2}\Delta_2|I_{\nu_2k_2}^z|^2\sum_n\left|\sum_{\gamma} L_{2\gamma}I_{k_2n}^{\gamma}\right|^2, \quad (21)$$

where $\Delta_i=\Delta(\omega_0-\omega_{\nu_ik_i},\Gamma_{\dot{\nu}_ik_i})$. If and only if the absorption strengths of the two channels are equal, i.e., $\Sigma_{\nu_1}\Delta_1|I_{\nu_1k_1}^z|^2=\Sigma_{\nu_2}\Delta_2|I_{\nu_2k_2}^z|^2=I_0$, then one has

$$\sigma(\omega',\omega_0)=I_0\sum_n\left(\left|\sum_{\gamma} L_{2\gamma}I_{k_1n}^{\gamma}\right|^2+\left|\sum_{\gamma} L_{2\gamma}I_{k_2n}^{\gamma}\right|^2\right) \quad (22)$$

and only in this case will the resonant x-ray emission have the same spectral line shape as that of the nonresonant spectrum. Therefore, in general, one should expect to see some difference between resonantly and nonresonantly excited x-ray emission spectra already for a system with two core levels, even though of different symmetry. It should be noted that this difference is not due to the interference between different scattering channels, but rather due to the polarization selective excitation, which necessitates an explicit consideration of the intermediate state.

It can be proven that the formula given above can be obtained from the so-called general two-step model (TSII).[6] In general, the TSII is equivalent to a one-step model without considering the interference effect.[6]

C. Interference: Two (near-degenerate) core levels of the same symmetry

We assume that the molecule has two (near-degenerate) core levels of the same symmetry, e.g., a_1. With the fixed polarization vector along z, only unoccupied orbitals with symmetry a_1 will be excited. For a system with one unoccupied orbital ν_1 with symmetry a_1, the excitation can involve either of the core levels and, as a consequence, the total amplitude must be computed as a summation of two individual channels $(i=1,2)$:

$$F_{\nu_1n}^{z\gamma}=F_{\nu_1n}^{z\gamma}(k_1)+F_{\nu_1n}^{z\gamma}(k_2), \quad (23)$$

$$F_{\nu_1n}^{z\gamma}(k_i)=\frac{D(k_i)}{\omega_0-\omega_{\nu_1k_i}+i\Gamma_{nu_1k_i}}, \quad (24)$$

$$D(k_i)=\alpha\omega_{\nu k_i}\omega_{nk_i}d_{\nu_1k_i}^z d_{k_in}^{\gamma}. \quad (25)$$

The cross section can be written

$$\sigma(\omega',\omega_0)\propto\sigma_1+\sigma_2+\sigma_{int} \quad (26)$$

and

$$\sigma_1 = \frac{D_{k_1}^2}{\delta\omega_{k_1}^2 + \Gamma^2}, \quad \sigma_2 = \frac{D_{k_2}^2}{\delta\omega_{k_2}^2 + \Gamma^2},$$

$$\sigma_{int} = 2D_{k_1}D_{k_2}\frac{\delta\omega_{k_1}\delta\omega_{k_2} + \Gamma^2}{(\delta\omega_{k_1}^2 + \Gamma^2)(\delta\omega_{k_2}^2 + \Gamma^2)}, \tag{27}$$

where $\delta\omega_{k_i} = \omega_0 - \omega_{\nu_1 k_i}$; the lifetimes of the two core-excited states are assumed to be the same. The cross section produced by the interference of the two channels, σ_{int}, is dependent on the energy separation between the two core levels. If one assumes $\delta\omega_{k_1} = 0$, i.e., resonant with one core-excited state, then $\delta\omega_{k_2} = \omega_{\nu_1 k_1} - \omega_{\nu_1 k_2} = \omega_{k_1 k_2}$, is the energy difference between the two core excited states, or the energy difference between the two core levels in the frozen picture. The interference term can be written as

$$\sigma_{int} = 2D_{k_1}D_{k_2}\frac{1}{\omega_{k1k2}^2 + \Gamma^2}, \tag{28}$$

i.e., the larger the energy separation, ω_{k1k2}, the smaller is the interference effect.

III. COMPUTATIONAL DETAILS

In order to evaluate the resonant x-ray emission cross sections, it is necessary to compute the dipole transition moments $d_{\nu k}^{\beta}$ and d_{kn}^{γ}, which correspond to excitations from the core orbital k to an unoccupied orbital ν and to the decay from the occupied orbital n into the core hole k, respectively.

The calculation of these matrix elements is in the present work performed in the framework of DFT using the Kohn-Sham self-consistent field (SCF) ground-state orbitals (DFT frozen); e.g., we include neither core-hole (initial state) nor valence-hole (final state) relaxation effects in the calculations of the intensities. The frozen orbital DFT approximation (DFT frozen)[19] has previously been applied to the calculations of nonresonant x-ray emission spectra for a group of both gas phase and chemisorbed molecules; together with the transition potential DFT method for the calculation of the valence level binding energies this procedure has proven to work very well for predicting nonresonant XES spectra. A discussion of the difference between frozen and relaxed nonresonant XES spectra was also made in connection with calculations performed in Ref. 26.

Calculations of the resonant and nonresonant x-ray emission spectra were carried out with the deMon program[27,28] which implements orbital-based density-functional theory. The present study uses a series of copper clusters to model the interaction of the ethylene with the (110) copper surface. For the smaller cluster models (up to Cu_{28}) the copper atoms were described at the all-electron level. For the larger cluster models, e.g., Cu_{50} and Cu_{86}, the central Cu_{14} subunit was described at the all-electron level and the surrounding atoms described using a one-electron effective core potential (ECP) model developed by Wahlgren and co-workers.[29] The core, including the $3d$ shell, is thus described by a static potential, which includes the effects of relaxation and polarization of the $3d$ orbitals, but only the $4sp$ valence electrons are treated explicitly.

Two different chemisorbed structures of benzene resulting from geometry optimization on cluster models of Cu(110) have previously been reported:[30] a distorted, inverted boat structure which requires an electronic excitation was found to be somewhat more strongly bound, while the planar, π-bound species with a slight bending up of the hydrogens was found somewhat less favored. From comparison of computed and theoretical XES and near-edge x-ray absorption fine-structure (NEXAFS) spectra[26] it was argued that the less distorted structure was observed in the experiment on benzene on Cu(110) while the more strongly distorted species could correspond to chemisorption on Ni and Mo substrates. In the present work only the less distorted form has been considered and only results for a medium-size cluster, Cu_{28}, will be presented.

The all-electron orbital basis set for Cu was that of Wachters[31] using an $[8s,5p,3d]$ contraction with one diffuse p function and one d function added. For hydrogen the primitive $(5s)$ basis set from Ref. 32 was used, augmented with one p function and contracted to $[3s1p]$, while for carbon triple-zeta valence plus polarization[33] (TZVP) was used in a generalized $[4s3p]$ contraction and with one added d function. These basis sets were used both for the optimization of the geometries and for the determination of the spectra. All calculations were done using the gradient corrected BP86 Refs. 34,35 exchange and correlation potentials.

A δ function is assumed for the incoming photon, corresponding to narrow-band excitation. The experimental value of 0.15 eV for the lifetime broadening of the core-excited states of carbon is used in the simulations.

IV. EXPERIMENT

The experiments were carried out at the IBM undulator beamline 8.0 at the Advanced Light Source, Lawrence Berkeley National Laboratory. The undulator beamline delivers almost completely linearly polarized synchrotron radiation (SR), which passes a modified spherical grating monochromator. The monochromatic SR is focused into a spot of $100\times100\,\mu m^2$ with a flux of $10^{13}-10^{14}$ photons/s. The endstation consists of two UHV chambers for sample preparation and analysis. The base pressure in the system was 1×10^{10} torr. The analyzer chamber is rotatable around an axis parallel to the incoming beam and houses an electron energy analyzer (Scienta SES200),[36] an x-ray emission spectrometer (both mounted perpendicular to the incoming beam), and a multichannel plate detector for x-ray absorption measurements. The x-ray emission spectrometer is a multigrating, grazing incidence spectrometer with a movable multichannel plate based detector described in detail elsewhere.[37] The spectrometer was set to a resolution of 0.5 eV. The photon energy resolution of the incoming light was set to 0.3 eV. Grazing and normal XE spectra were recorded by rotation of the spectrometer chamber keeping the excitation energy fixed.

The measurements on C_2H_4/Cu(110) were performed with resonant excitation at 284.8 eV and off-resonant excitation at 288.8 eV. The E vector of the incident SR was perpendicular to the surface normal in all measurements. The sample was moved automatically during the measurements at a rate fast enough to avoid beam damage. No changes in the

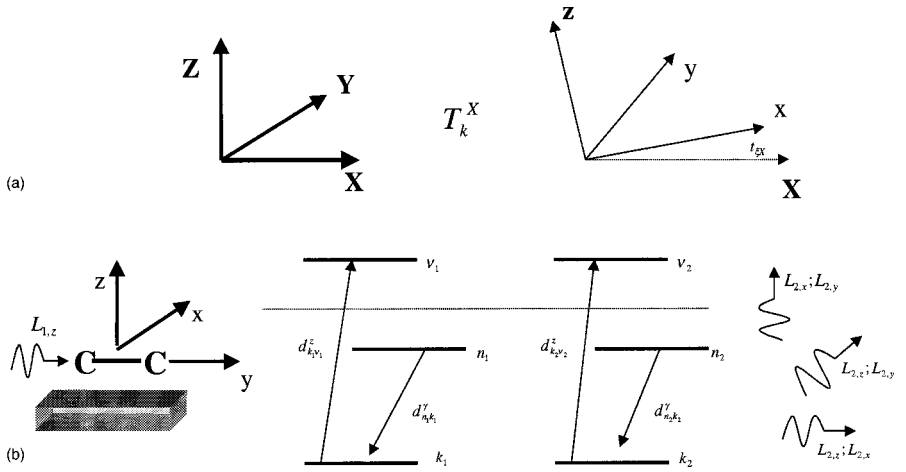

FIG. 1. (a) Transformations between laboratory and molecular coordinate frames. (b) Matrix elements of the RIXS cross section for the case of two core orbitals (symmetry related centers) of a_1 and b_1 symmetry.

*C*1*s* XPS spectrum were found before and after XE measurement. All spectra were energy calibrated by measuring elastically scattered light at two different incoming energies. The monochromater was calibrated using the fact that the difference in kinetic energies of photoelectrons excited by first and second order is exactly the photon energy.

Two Cu(100) crystals of 1 cm diameter each were mounted on the sample holder, where temperatures between 40 and 1500 K can be achieved. The crystals were cleaned by cyclic argon ion sputtering and annealing to 900 K until a well-ordered low-energy electron diffraction (LEED) pattern was obtained and no surface contaminants were observed with XPS. The LEED pattern of the two crystals also verified their respective azimuthal orientations. Saturated C_2H_4 monolayers on Cu(110) were prepared by dosing 2 L onto the sample at 80 K and was monitored with XPS.

Relative to each other the crystals were rotated 90° around the [110] surface normal. Thus one crystal had the [001] axis parallel to the incoming beam and the other the $[1\bar{1}0]$ axis. As the direction of detection was varied from normal to grazing emission, states of different orbital symmetry could be separated. In normal emission geometry XE was observed along the [110] axis. In grazing emission geometry different directions of observation were achieved for the two different Cu(110) crystals. For one crystal XE along the [001] axis was observed, whereas for the other XE along the $[1\bar{1}0]$ axis was measured.

The experimental data on benzene on Cu(110) have been taken from Ref. 22 where the detailed description of the experiment may be found.

For ethylene on Cu(110) the x-ray emission spectra are obtained from three measurements along three different directions, as shown in Fig. 1.

$$I_1 = I_x + I_y, \quad I_2 = I_y + I_z, \quad I_3 = I_x + I_z. \tag{29}$$

V. RESULTS AND DISCUSSION

The geometric structure of ethylene chemisorbed on Cu(110) has earlier[30] been optimized at the DFT level using energy gradients. The ethylene/Cu(110) cluster model has the ethylene molecule chemisorbed in the di-σ orientation, placed with the C-C axis parallel to the nearest Cu-Cu neighbor pair on the substrate. For this surface, the C-C distance becomes 1.39 Å, which is 0.06 Å larger than the computed C-C distance in the gas phase ethylene molecule, while the hydrogens move upward from the surface.[30]

The ground-state ethylene molecule in the gas phase belongs to the D_{2h} symmetry group and the electronic configuration is $(1a_g)^2(1b_{1u})^2(2a_g)^2(2b_{1u})^2(1b_{2u})^2(3a_g)^2(1b_{3g})^2(1b_{3u})^2\ ^1A_g$. The lowest unoccupied molecular orbital (LUMO) is $1b_{2g}$. When electronic dipole transitions are considered, one expects strict parity selection rules to apply for the resonant spectra. For instance, in the case of LUMO excitation, only emission from gerade orbitals should be observable. Due to the interaction with the surface, the adsorbed ethylene reduces to C_{2v} symmetry with the electronic configuration, $1a_1^2 1b_1^2 2a_1^2 2b_1^2 1b_2^2 3a_1^2 1a_2^2 4a_1^2\ ^1A_1$. The LUMO then transforms according to b_1 symmetry, but quite a few new orbitals close in energy to the LUMO of ethylene appear due to the bonding to the substrate. The adsorbed ethylene molecule studied here, with two core orbitals of different symmetry, corresponds to the case discussed in Sec. II B. The polarization of the incoming photon is considered parallel to the *z* axis, which contains the direction of the surface normal vector (see Fig. 1). The applicable equation to describe this case in the simulations is thus Eq. (21) as given above.

A. Ethylene on copper

1. Cluster convergence

We use here a cluster model to simulate the surface and it is relevant to discuss first the convergence of spectra in terms of cluster size. In Fig. 2, both nonresonant and resonant x-ray emission spectra have been computed for different cluster models. For the resonant case, the 284 eV excitation is simulated by considering excitations into the first unoccupied molecular orbital (LUMO).

The nonresonant spectra have been calculated using the traditional two-step model, in which the absorption strength is assumed to be a constant and where only the decay from occupied valence orbitals to the core hole is considered. Equation (22) then holds, providing information only on the valence orbitals of the system. On the other hand, the resonant spectra can give additional information about the unoccupied orbitals. Figure 2 gives a general idea about the cluster convergence of the computed spectra and it is clear that for the nonresonant spectra the differences between having 24, 50, or 86 copper atoms in the cluster are not really sig-

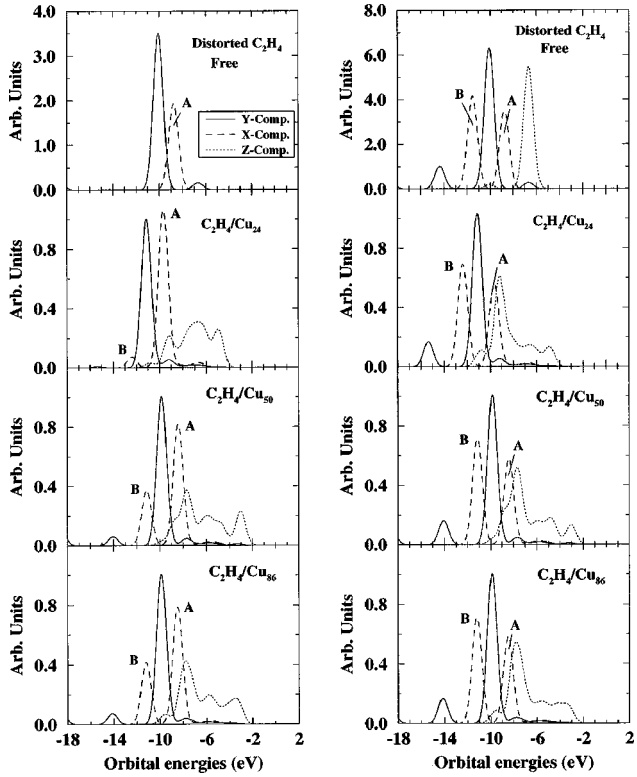

FIG. 2. Cluster convergence of $C(1s)$ resonant (left) and nonresonant XES (right) of chemisorbed ethylene on Cu(110). Calculations are performed at DFT(BP86) level with the program DeMon (Ref. 28).

nificant, indicating a fast convergence of the relevant part of the valence bands. For the resonant spectra there are significant differences between spectra generated from the two smaller cluster models; for instance, the intensity ratio of the two peaks in the X direction as well as the intensity distribution in the Z direction, while the differences between having 50 or 86 atoms is minor. The greater sensitivity of the resonant spectra is a consequence of their dependence on the description of the unoccupied orbitals, especially those orbitals resulting from the surface bonding.

2. Polarization and symmetry selectivity

As shown in Sec. II B, and further discussed here, the polarization selectivity is responsible for the differences between the resonant and nonresonant spectra. Due to the fixed orientation of the adsorbates, only certain orbitals can be observed along certain directions. The relation between the polarization vector and symmetry of observable valence orbitals for chemisorbed ethylene is summarized in Table I.

If free ethylene is considered in the distorted geometry, e.g., the chemisorbed geometry without substrate, we then remove the contributions due to the bonding of ethylene to the surface (see Fig. 2). Therefore, Eq. (21) can be simply written for one channel, in this case for the b_1 excitations and one obtains

$$\sigma(\omega',\omega_0)=\Delta_{b_1}|I^z_{nb_1 1b_1}|^2\sum_n\left|\sum_\gamma L_{2\gamma}I^\gamma_{1b_1 n}\right|^2, \quad (30)$$

i.e., only the emission from valence orbitals to one of the core holes, the $1b_1$ orbital is observed. In C_{2v} symmetry

TABLE I. The relationship between polarization vector of emitted light and the symmetry allowed emission orbitals for nonresonant and resonant X-ray emission spectra of physically and chemically adsorbed ethylene.

Polarization vector	Symmetry allowed emission orbitals		
	Nonresonant	Resonant	
		Physical	Chemical
X	a_1,b_1	a_1	a_1,b_1
Y	a_2,b_2	a_2	a_2,b_2
Z	b_1,a_1	b_1	b_1,a_1

b_1-b_2 transitions are forbidden and so emission from the $1b_2$ valence level is not observed. Such a symmetry selectivity is a unique feature for adsorbates, resulting from the combination of the polarization selective absorption and fixed orientation of the adsorbed molecule. Furthermore, comparing with the corresponding nonresonant case, emission from a smaller number of orbitals can be observed along a certain detection direction, as shown in Table I.

Adding the substrate one introduces surface chemical bonds, which for hydrocarbon molecules are obtained by mixing the π and π^* with the metal bands. However, C_{2v} symmetry is still preserved and the polarization selective absorption discussed in Sec. II B is still valid. According to the calculations, two sets (nb_1,ma_1) of unoccupied orbitals of symmetry b_1 and a_1, respectively, contribute to the absorption process. The nb_1 orbitals have the character of LUMO of ethylene mixed with metal orbitals, whereas the ma_1 orbitals have character of the HOMO of ethylene mixed with metal orbitals. Equation (21) can then be rewritten as

$$\sigma(\omega',\omega_0)=\Delta_{a_1}|I^z_{ma_1 1a_1}|^2\sum_n\left|\sum_\gamma L_{2\gamma}I^\gamma_{1a_1 n}\right|^2 + \Delta_{b_1}|I^z_{nb_1 1b_1}|^2\sum_n\left|\sum_\gamma L_{2\gamma}I^\gamma_{1b_1 n}\right|^2. \quad (31)$$

Comparing the free ethylene molecule with the structure of the chemisorbed specie, the appearance of the ma_1 states opens up a new transition channel, namely, emission from the valence to the core hole $(1a_1)$ of a_1 symmetry. Now, the b_2 states become observable since the transition a_1 to b_2 is dipole allowed [peak B in Fig. 2(a)]. The relationship between the symmetry allowed emission states and polarization direction of the emitted light is the same as that for the nonresonant case. However, the spectral distribution is not necessarily the same for the two cases. Here, we use the X component of the emission spectra to illustrate this point.

In the X component of the emission spectra [Figs. 2(a) and 2(b)], there are two main peaks, A and B, resulting from two different scattering channels through two different intermediate unoccupied orbitals, namely, the nb_1 and ma_1 orbitals. The intensity ratio, I_A/I_B, of the two peaks A and B, is controlled by the ratio

$$R_x^{\mathrm{res}}=\frac{[\Delta_{b_1}|I^z_{nb_1 1b_1}|^2|I^x_{1b_1 a_1}|^2]}{[\Delta_{a_1}|I^z_{ma_1 1a_1}|^2|I^x_{1a_1 b_1}|^2]}, \quad (32)$$

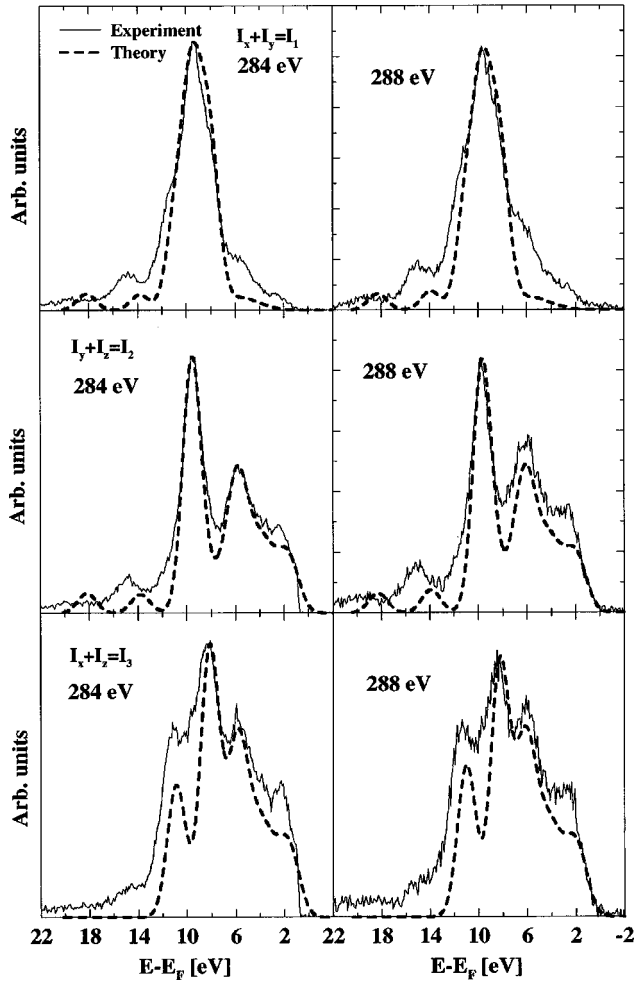

FIG. 3. Comparison with experiment for two different excitation energies. C_2H_4/Cu_{86}, FWHM=1.0 eV.

$$R_x^{\mathrm{non}}=\frac{[|I^x_{1b_1a_1}|^2]}{[I^x_{1a_1b_1}|^2]}. \tag{33}$$

If $R_x^{\mathrm{res}}=R_x^{\mathrm{non}}$, i.e., $\Delta_{b_1}|I^z_{nb_11b_1}|^2=[\Delta_{a_1}|I^z_{ma_11a_1}|^2$, then the nonresonant and the resonant spectra will be the same.

For the small clusters, like Cu_{24}, there are no near-degeneracy effects involving the excitation into the unoccupied ma_1 and nb_1 sets, i.e., the factor Δ_{a_1} is small, which, together with the fact that the transition dipole between the core hole and the ma_1 orbitals is also quite small, gives a ratio R_x^{res} much larger than R_x^{non} and consequently a small intensity for peak *B*. Increasing the size of the cluster, both the energy differences and transition moments become more similar such that the ratio R_x^{res} decreases and so does the intensity of peak *B*. For the largest cluster model, Cu_{86}, $R_x^{\mathrm{res}}=1.45R_x^{\mathrm{non}}$. The final resonant spectrum should differ from the nonresonant one, as indicated in Fig. 2. A similar analysis can be applied for the *Y* and *Z* components of the spectra.

3. Experimental comparison

Figures 3(a) and 3(b) show the comparison of the computed and experimental spectra for the two different excitation energies, where the results for the largest cluster model are shown. The experiment is only weakly photon energy dependent as noted in previous sections. Most, if not all, salient structures of the experimental spectra are reproduced by the simulations. The experimental spectra will contain additional broadening due to vibrational excitations and finite lifetimes of the final valence hole states not taken into account in the simulations. The intensities of the new states due to the surface bonding are somewhat underestimated. This seems also to be the case for the high-binding-energy side of the three components.

There can be several possible reasons for these discrepancies, where one possibility is the exclusions of the vibrational motions in the present simulations. A second possibility is that, in the present high-coverage situation, the adsorbed ethylenes tilt somewhat away from the substrate in order to minimize the repulsion against neighboring adsorbates.

Figure 3(a) shows the computed resonant x-ray emission spectrum at 288 eV for the Cu_{86} cluster model. This energy is only 4 eV from the LUMO excitation and it should be treated as a resonant process. As shown in Fig. 3(a), the resonant spectrum at 288 eV is very similar to that at energy of 284 eV, but quite different from the nonresonant spectra. The 288-eV photon energy was chosen to avoid any initial-state satellites, which would complicate the spectrum. This is generally seen for excitations well above threshold, where nondiagram transitions start to appear.[38]

4. Surface bonding

Since there is a good agreement between the experimental and theoretical spectra we use the calculations to shed more light on the electronic states of importance to the surface chemical bond. Figure 4 shows a decomposition of the spectra into valence states of different symmetry. The *x* and *y* components correspond to the σ orbitals and are essentially unchanged compared with a free distorted ethylene molecule. The *z* component, involving the π orbital, shows the appearance of new electronic states. The valence states of a_1 symmetry correspond to the intramolecular bonding π orbital and the valence states of b_1 symmetry to the antibonding π^* orbital.

To the low-energy side one can see a peak at 7.4 eV, which belongs to symmetry ''a_1''. This peak is also seen in the free, distorted ethylene, but it is not seen in the gas phase ethylene.[19] Therefore, one could argue that this peak is a consequence of the internal distortion of the ethylene upon adsorption. The same applies to the feature located around 5.5 eV in the *Y* component.

The features from 6-eV binding energy and up to the Fermi level in the *Z* component are obviously due to the surface chemical bond. This region can be divided into three sets of bonding orbitals: the first with highest binding energy (6.5–4.5 eV) contains more π ($1b_{2u}$) character, the second below 2.5 eV up to the Fermi level more π^* ($1b_{3g}$) character and the third, which corresponds to the intermediate region between 4.5 and 2.5 eV has similar contributions from the π and the π^* orbitals. In these three regions one also finds the contributions from the 3*d* metal band.

At this point it is relevant to bring into the discussion the interaction mechanism revealed in the present study and put

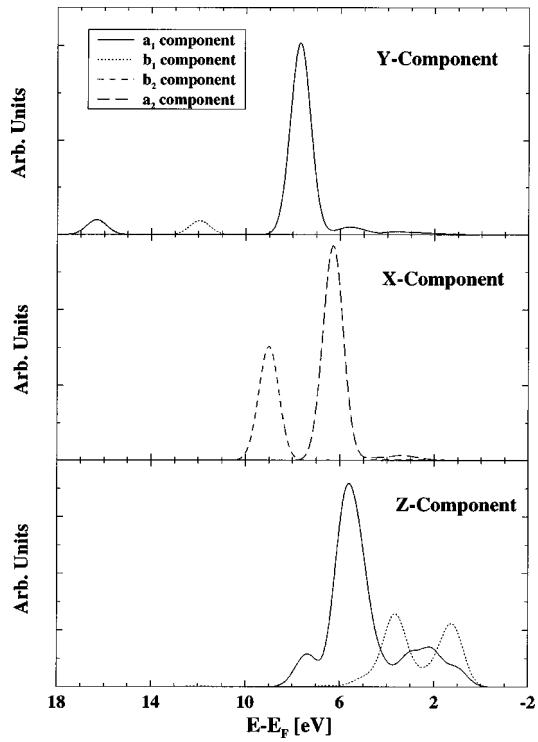

FIG. 4. Analysis of the emission components of the resonant XES calculation of C_2H_4/Cu_{86}.

it in the context of the molecular frontier orbital approach to the bonding of this π complex, i.e., the Dewar, Chatt, and Duncanson bonding model[39,40] and the spin-uncoupling mechanism proposed in Ref. 30. In the Dewar, Chatt, and Duncansson model the π system donates charge into unoccupied levels of the metal while the π^* orbital of the adsorbate becomes occupied through back donation.

This picture could be seen as the end point in the spin-uncoupling mechanism. In the latter, the adsorbate is bond prepared by an explicit $\pi \rightarrow \pi^*$ triplet excitation, which is induced by the interaction with the metal surface leading to rehybridization in the adsorbate and preparing the molecule to form direct covalent bonds with the metal orbitals.

These covalent bonds are formed by combining the π and π^* orbitals of the adsorbate with the metal orbitals, namely, $3d$ and $4s$, yielding a new set of bonding and antibonding orbitals as reflected in the calculations and ''seen'' in the experiment (compare Figs. 2 and 3). We can anticipate that the occupied part of the π^* orbitals form bonding states with the Cu $3d$ and $4s$ orbitals constituting the two peaks seen in Fig. 4. The corresponding antibonding states will form the π^* resonance above the Fermi level, which was used to generate the core-excited state at 284 eV. The π orbital interacting in a bonding fashion will constitute the main peak at 5.5 eV. The reduction upon adsorption of the symmetry selective intensity variation at the π^* resonance is a result of contributions of π orbitals being pushed above the Fermi level. These states will most likely correspond to the antibonding π states. The amount of π and π^* character in the different regions of the spectra (Z component) are then determined by the energy difference between these two orbitals and the center of each metal band.

B. Benzene

X-ray emission of free and adsorbed benzene have been presented and analyzed on several occasions previously. Experimental nonresonant and resonant spectra were given in Refs. 41 and 15, respectively, for free benzene and in Ref. 22 for benzene on copper and nickel surfaces. Theoretical analyses have been carried out for the nonresonant case by means of DFT (Ref. 19) and Hartree-Fock[26] techniques. The bonding to the surface has also been analyzed in conjunction with spectral XE analysis[22] and by several other characterization techniques, see e.g., Refs. 42–44. $C_6H_6/Cu(110)$ also served as a test for the concept of spin uncoupling by the present authors.[30] For the various aspects of bonding, electronic and geometric structure of this system we refer to these previous works; here the focus will be on the importance of the channel interference effect to predict the *resonant* x-ray emission spectra, and to understand the salient differences with respect to the nonresonant counterpart.

1. Interference effects

Benzene is a good prototype molecule for illustrating the effect of interference in the resonant x-ray emission. Benzene belongs to the D_{6h} symmetry group and the resonant x-ray emission is governed by the parity selection rules. Such selection has indeed been observed in that the HOMO ($1e_{1g}$) of benzene disappears in x-ray emission at the LUMO (e_{2u}) excitation.[15]

Analyzing surface adsorbed benzene it is relevant to make analogy with the case of monosubstituted benzene, for which the molecular symmetry is also lowered to C_{2v} symmetry. No parity selection or symmetry selection rule exists for x-ray Raman transitions involving isolated nonoccupied levels in a molecule with such a low symmetry. However, due to that the chemical shifts of the different core-excited $C1s$-π^* states can be small, in the order of the lifetime width, an interference effect may operate so that the intensity of certain transitions may be quenched in the resonant x-ray emission. The smaller the shifts, the more benzene-like becomes the resonant spectrum due to the interference.[16]

For the adsorbate, the presence of the surface breaks the inversion symmetry of the gas phase benzene. The interaction between the benzene molecule and the surface furthermore results in a geometry distortion; on the Cu(110) surface, it has C_{2v} symmetry with nondegenerate core orbitals. The situation is thus similar to substituted benzenes, and one can expect strong interference effects from the decay of the ''chemically shifted'' $C1s$-π^* intermediate states.

For benzene on Cu(110), the six core orbitals can be represented as two a_1, two b_1, one a_2 and one b_2 orbital. For an excitation along the z axis, the unoccupied orbitals with symmetries a_1, b_1, a_2, and b_2 can all be excited. There is therefore no symmetry discrimination due to the dipole selection rule, i.e., all orbitals are allowed. In accordance with the discussion in Sec. II B, we can see that interference is due to the channels involving core orbitals with the same symmetry, i.e., the two a_1 to the two b_1 core orbitals, respectively, in the case of benzene on a surface.

Figure 5 presents the resonant x-ray emission spectrum at an excitation energy corresponding to the first π^* level. The spectra are decomposed into π and σ contributions. For each

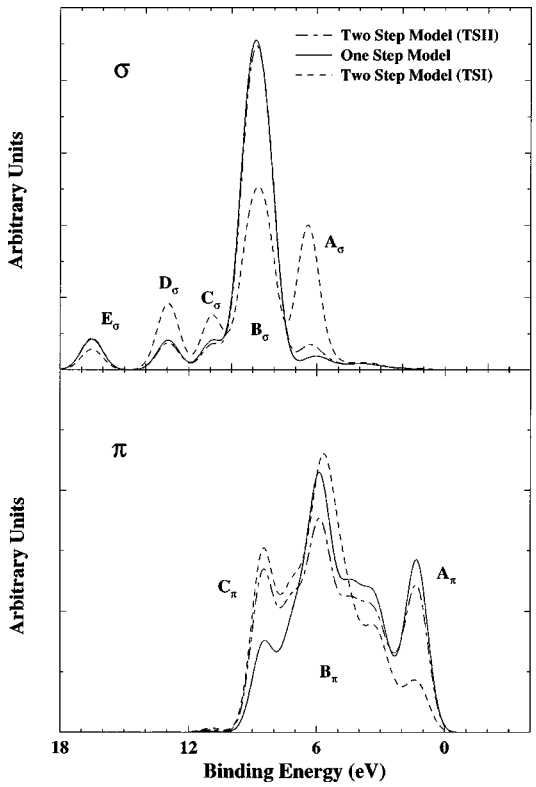

FIG. 5. $C(1s)$ XES of chemisorbed benzene on Cu(110). Comparison of the one- and two-step models.

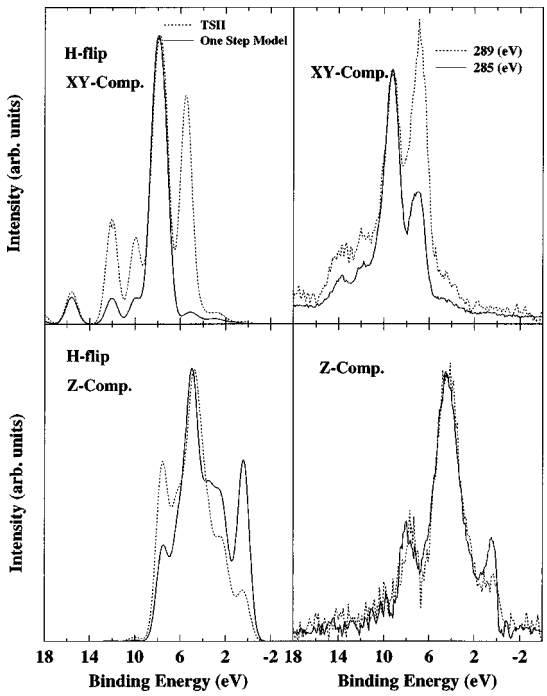

FIG. 6. Comparison of the theoretical spectra (left) with experiment (right) for two different exciting photon energies. C_6H_6/Cu_{28}.

component, we present three spectra calculated from the two different two-step models, TSI, TSII, and from the one-step model.

For the π component, there are three main features in the spectra, named A_π, B_π, and C_π. The TSI model describes the decay of the valence levels accounting for neither polarization nor interference effects, while the TSII model takes into account the polarization selectivity of the resonant x-ray emission. It is clearly shown by Fig. 6 that the polarization selectivity has a large effect on the A_π feature, and a small effect on the C_π feature. The variation of the A_π feature thus indicates that the levels related to surface bonding are sensitive to the polarization properties of excitation and emission. The inclusion of interference effects introduces significant further changes in the spectrum, see Fig. 6.

For the σ component, five distinct features, A_σ, B_σ, C_σ, D_σ, and E_σ are resolved. Major changes are introduced by the inclusion of the polarization selectivity, i.e., the spectrum from the TSII model is significantly different from that of TSI. The relative intensities of features C_σ, D_σ and, especially, A_σ are reduced, and the intensity of feature B_σ is increased compared to the two-step model TSI. Further, considering the interference through the one-step model, the intensity of feature A_σ is almost depleted. It is interesting to note that for free benzene, feature A_σ, assigned as due to the $3e_{2g}$ level, is a dipole forbidden orbital for LUMO excitations.[15] This symmetry selection rule seems to become reinforced by the interference effects.

2. Experimental comparison

In Fig. 6 we compare results from simulations using the two-step TSII and the one-step models with experimental data. The latter spectra are obtained at 285 and 289 eV, here representing (LUMO) resonant and nonresonant excitation, respectively.

The major difference between the two models, namely, the interference contributions, seems to be repeated to a certain extent when comparing with the difference of the two experimental spectra. The most salient change is the lowering of the ''A_σ'' ($3e_{2g}$) intensity. Thus the experimental comparison indeed seems to support the notion that channel interference depletes this structure and that it reinforces a symmetry selection rule.

The π symmetry spectra are somewhat harder to evaluate, partly because having only 3–4 features available—mainly due to the $1a_{2u}$, $1e_{1g}$, and $1e_{2u}$ levels—the outcome of the experimental comparison becomes somewhat dependent on the normalization procedure. However, the relative decrease of the $1e_{1g}$ to $1e_{2u}$ intensity ratio seems to be accounted for by the channel interference effect, on the other hand the a_{2u} to $1e_{1g}$ change is not (see, however, discussion below).

VI. SUMMARY

In this work a theory was presented for resonant emission spectra, or Raman spectra, in the soft-x-ray wavelength region, for strictly ordered surface adsorbed molecules, with special emphasis on symmetry and polarization selectivity and the role of interference. Results from density-functional simulations and new experimental data for ethylene and benzene on a copper surface were presented and analyzed, and served to test the theory.

The cluster model approach was used to model the interaction of the molecule with the surface and for the computation of the spectra. The model used for the calculation of the resonantly excited x-ray emission spectra of surface-adsorbate systems has the same complexity as for the non-

resonant emission spectra; the former are, however, more demanding with respect to convergence with cluster size. The larger sensitivity for the resonant spectra is a consequence of their dependence on the description of the virtual orbitals.

The ethylene and benzene cases represent well the two fundamental aspects of x-ray emission spectra we wished to study: symmetry and polarization selectivity and the role of interference. The experimental spectra show a subtle but significant dependence on the exciting photon energy, which, in the particular case of chemisorbed ethylene, is due to polarization selective excitation and not to interference of different scattering channels. The ethylene on copper RIXS spectrum shows strong polarization (or directional) selectivity in that *X,Y,Z* component spectra are quite different. There is thus strong entanglement between the symmetry of the emitting levels and the polarization (or direction) of the corresponding outgoing photon. In the case of benzene the shift among the core levels induced by surface adsorption leads to interference effects in the decay. Such interference is shown to alter the spectra substantially and restore some of the symmetry selectivity of the free species.

New states appear in the emission spectra of the adsorbates not present in the free molecule. Some dependence of the appearance of these states on the excitation energy is observed. In terms of the chemical bond, this may be understood as large mixing of π and π^* with the metal orbitals upon adsorption. This interaction and the peaks revealed in the spectra can be interpreted in terms of the spin-uncoupling mechanism proposed in Ref. 30 or the traditional Dewar-Chatt-Duncanson model.[39,40]

The results of the present work should be qualified with respect to some complicating aspects. Resonant x-ray emission, like other two-photon processes in general, can be strongly dependent on nuclear motion and vibronic coupling. Such coupling, not considered at all in this work, actually leads to symmetry breaking of electronic selection rules in some parts of the RIXS spectra of free benzene[15] and free ethylene.[45] Different hydrocarbons behave differently, for instance, in RIXS spectra of free acetylene symmetry selectivity is preserved to a large extent, while in ethane it is completely broken at resonance.[45] It is known that the coupling and the symmetry breaking is strongly dynamic, i.e., frequency dependent, and that it can be quenched by detuning the frequency from resonance, thereby restoring the symmetry selection rules.[46,45] It is still an open question whether the presence of the surface quenches or enhances such coupling, and if the dynamic features evident for the free species are observable also for adsorbates.

[1] J. J. Sakurai, *Advanced Quantum Mechanics* (Addison-Wesley, New York, 1967).

[2] T. Åberg and B. Grasemann, in *Resonant Anomalous X-Ray Scattering. Theory and Applications*, edited by G. Materlik, C. J. Sparks, and K. Fischer (North-Holland, Amsterdam, 1994), p. 431.

[3] G. B. Armen and H. Wang, Phys. Rev. A **51**, 1241 (1995).

[4] F. Kh. Gel'mukhanov and H. Ågren, Phys. Rev. A **49**, 4378 (1994).

[5] Y. Luo, H. Ågren, and F. K. Gel'mukhanov, J. Phys. B **27**, 4169 (1994).

[6] Y. Luo, H. Ågren, and F. Kh. Gel'mukhanov, Phys. Rev. A **53**, 1340 (1996).

[7] F. Gel'mukhanov, L. N. Mazalov, and N. A. Shklyaeva, Zh. Eksp. Teor. Fiz. **71**, 960 (1976) [Sov. Phys. JETP **44**, 504 (1977)].

[8] Y. Ma, Phys. Rev. B **49**, 5799 (1994).

[9] P. L. Cowan, in *Resonant Anomalous X-Ray Scattering. Theory and Applications*, edited by G. Materlik, C. J. Sparks, and K. Fischer (North-Holland, Amsterdam, 1994), p. 449.

[10] R. H. Pratt, L. Kissel, and Jr. P. M. Bergstrom, in *Resonant Anomalous X-Ray Scattering. Theory and Applications*, edited by G. Materlik, C. J. Sparks, and K. Fischer (North-Holland, Amsterdam, 1994), p. 9.

[11] H. Ogasawara, A. Kotani, and B. T. Thole, Phys. Rev. B **50**, 12 332 (1994).

[12] J. A. Carlisle, E. L. Shirley, E. A. Hudson, L. J. Terminello, T. A. Callcott, J. J. Jia, D. L. Ederer, R. C. C. Perera, and F. J. Himpsel, Phys. Rev. Lett. **74**, 1234 (1995).

[13] M. Weinelt, A. Nilsson, M. Magnuson, T. Wiell, N. Wassdahl, O. Karis, A. Föhlisch, N. Mårtensson, J. Stöhr, and M. Samant, Phys. Rev. Lett. **78**, 967 (1997).

[14] F. Gel'mukhanov and H. Ågren, Phys. Rev. B **57**, 2780 (1998).

[15] P. Skytt, J. H. Guo, N. Wassdahl, J. Nordgren, Y. Luo, and H. Ågren, Phys. Rev. A **52**, 2572 (1995).

[16] Y. Luo, H. Ågren, J. H. Guo, P. Skytt, N. Wassdahl, and J. Nordgren, Phys. Rev. A **52**, 3730 (1995).

[17] Y. Luo, H. Ågren, F. Kh. Gel'mukhanov, J. H. Guo, P. Skytt, N. Wassdahl, and J. Nordgren, Phys. Rev. B **52**, 14 478 (1995).

[18] F. Gel'mukhanov and H. Ågren, J. Chem. Phys. **109**, 5060 (1998).

[19] L. Triguero, L. G. M. Pettersson, and H. Ågren, J. Phys. Chem. A **102**, 10 599 (1998).

[20] A. Nilsson, P. Bennich, T. Wiell, N. Wassdahl, N. Mårtensson, J. Nordgren, O. Björneholm, and J. Stöhr, Phys. Rev. B **51**, 10 244 (1994).

[21] A. Nilsson, M. Weinelt, T. Wiell, P. Bennich, O. Karis, N. Wassdahl, J. Stöhr, and M. Samant, Phys. Rev. Lett. **78**, 2847 (1997).

[22] M. Weinelt, N. Wassdahl, T. Wiell, O. Karis, J. Hasselström, P. Bennich, A. Nilsson, J. Stöhr, and M. Samant, Phys. Rev. B **58**, 7351 (1998).

[23] Y. Luo, O. Vahtras, F. K. Gelmukhanov, and H. Ågren, Phys. Rev. A **55**, 2716 (1997).

[24] P. Glans, K. Gunnelin, P. Skytt, J.-H. Guo, N. Wassdahl, J. Nordgren, H. Ågren, F. Gel'mukhanov, T. Warwick, and E. Rotenberg, Phys. Rev. Lett. **76**, 2448 (1996).

[25] P. Skytt, P. Glans, K. Gunnelin, J.-H. Guo, J. Nordgren, Y. Luo, and H. Ågren, Phys. Rev. A **55**, 134 (1997).

[26] L. G. M. Pettersson, H. Ågren, Yi Luo, and L. Triguero, Surf. Sci. **408**, 1 (1998).

[27] A. St-Amant and D. R. Salahub, Chem. Phys. Lett. **169**, 387 (1990).

[28] D. R. Salahub, R. Fournier, P. Mlynarski, I. Papai, A. St-Amant, and J. Ushio, in *Density Functional Methods in Chemistry*, edited by J. Labanowski and J. Andzelm (Springer, New York,

1991), p. 77; A. St-Amant, Ph.D. thesis, Université de Montréal, 1992. The present version of the program has been substantially modified by L. G. M. Pettersson.
[29] A. Mattsson, I. Panas, P. Siegbahn, U. Wahlgren, and H. Åkeby, Phys. Rev. B **36**, 7389 (1987).
[30] L. Triguero, L. G. M. Pettersson, B. Minaev, and H. Ågren, J. Chem. Phys. **108**, 1193 (1998).
[31] A. J. H. Wachters, J. Chem. Phys. **52**, 1033 (1970).
[32] S. Huzinaga, J. Chem. Phys. **42**, 1293 (1965).
[33] T. H. Dunning, Jr., J. Chem. Phys. **55**, 716 (1971).
[34] A. D. Becke, Phys. Rev. A **38**, 3098 (1988).
[35] J. P. Perdew, Phys. Rev. B **33**, 8822 (1986).
[36] N. Mårtinsson, P. Baltzer, P. Brühwiler, J. O. Forsell, A. Nilsson,A. Stenborg, and B. Wannberg, J. Electron Spectrosc. Relat. Phenom. **70**, 117 (1994).
[37] J. Nordgren, G. Bray, S. Cramm, R. Nyholm, J. E. Rubensson, and N. Wassdahl, Rev. Sci. Instrum. **60**, 1690 (1989).
[38] P. Bennich, T. Wiell, N. Wassdahl, and A. Nilsson (unpublished).
[39] M. J. S. Dewar, Bull. Soc. Chim. Fr. **18**, C79 (1951).
[40] J. Chatt and L. A. Duncanson, J. Chem. Soc. **1953**, 2939.
[41] J. Nordgren, L. Selander, L. Pettersson, R. Brammer, M. Bäckström, C. Nordling, and H. Ågren, Phys. Scr. **27**, 169 (1983).
[42] J. R. Lomas, C. J. Baddeley, M. S. Tikhov, and R. M. Lambert, Langmuir **11**, 3048 (1995).
[43] J. R. Lomas, C. J. Baddeley, M. S. Tikhov, and R. M. Lambert, Chem. Phys. Lett. **263**, 591 (1996).
[44] D. P. Woodruff, in *Chemisorption and Reactivity of Supported Cluster and Thin Films: Towards an Understanding of Microscopic Processes in Catalysis,* edited by R. M. Lambert and G. Pacchioni (Kluwer Academic, MA, 1997), p. 193.
[45] K. Gunnelin *et al.* (unpublished).
[46] A. Cesar, F. Gel'mukhanov, Y. Luo, H. Ågren, P. Skytt, P. Glans, J.-H. Guo, K. Gunnelin, and J. Nordgren, J. Chem. Phys. **106**, 3439 (1997).